nanomaterials

MDPI

Article

Plasma-Etched Vertically Aligned CNTs with Enhanced Antibacterial Power

Emily Schifano [1,2], Gianluca Cavoto [3,4], Francesco Pandolfi [4], Giorgio Pettinari [5], Alice Apponi [6], Alessandro Ruocco [6], Daniela Uccelletti [1,2] and Ilaria Rago [3,4,*]

1 Dipartimento di Biologia e Biotecnologia "C. Darwin", Sapienza University of Rome, Piazzale Aldo Moro 5, 00185 Rome, Italy
2 SNN Lab, Sapienza Nanotechnology & Nano-Science Laboratory, Sapienza University of Rome, 00100 Rome, Italy
3 Dipartimento di Fisica, Sapienza University of Rome, Piazzale Aldo Moro 2, 00185 Rome, Italy
4 INFN Sezione di Roma, Piazzale Aldo Moro 2, 00185 Rome, Italy
5 Istituto di Fotonica e Nanotecnologie, CNR-IFN, Via del Fosso del Cavaliere 100, 00133 Rome, Italy
6 Dipartimento di Scienze, Università Degli Studi Roma Tre and INFN Sezione di Roma Tre, Via della Vasca Navale 84, 00146 Rome, Italy
* Correspondence: ilaria.rago@uniroma1.it

Abstract: The emergence of multidrug-resistant bacteria represents a growing threat to public health, and it calls for the development of alternative antibacterial approaches not based on antibiotics. Here, we propose vertically aligned carbon nanotubes (VA-CNTs), with a properly designed nanomorphology, as effective platforms to kill bacteria. We show, via a combination of microscopic and spectroscopic techniques, the ability to tailor the topography of VA-CNTs, in a controlled and time-efficient manner, by means of plasma etching processes. Three different varieties of VA-CNTs were investigated, in terms of antibacterial and antibiofilm activity, against *Pseudomonas aeruginosa* and *Staphylococcus aureus*: one as-grown variety and two varieties receiving different etching treatments. The highest reduction in cell viability (100% and 97% for *P. aeruginosa* and *S. aureus*, respectively) was observed for the VA-CNTs modified using Ar and O_2 as an etching gas, thus identifying the best configuration for a VA-CNT-based surface to inactivate both planktonic and biofilm infections. Additionally, we demonstrate that the powerful antibacterial activity of VA-CNTs is determined by a synergistic effect of both mechanical injuries and ROS production. The possibility of achieving a bacterial inactivation close to 100%, by modulating the physico-chemical features of VA-CNTs, opens up new opportunities for the design of self-cleaning surfaces, preventing the formation of microbial colonies.

Keywords: carbon nanotubes; chemical vapor deposition; antimicrobial; plasma etching; nanomorphology

Citation: Schifano, E.; Cavoto, G.; Pandolfi, F.; Pettinari, G.; Apponi, A.; Ruocco, A.; Uccelletti, D.; Rago, I. Plasma-Etched Vertically Aligned CNTs with Enhanced Antibacterial Power. *Nanomaterials* **2023**, *13*, 1081. https://doi.org/10.3390/nano13061081

Academic Editors: Jakob Birkedal Wagner and Krasimir Vasilev

Received: 1 February 2023
Revised: 1 March 2023
Accepted: 14 March 2023
Published: 16 March 2023

1. Introduction

Antibiotics, because of their affordable costs and quick action, are the main treatment of bacterial infections. In response, bacteria have developed the ability to evolve rapidly through mutations, becoming resistant to these treatments. In addition, bacterial species can transfer drug-resistant genes to each other through horizontal gene transfer, which is the acquisition of foreign genes by an organism [1]. This results in the emergence of multidrug-resistant (MDR) bacteria [2], an increasing trend due to the amplified use of antibiotics, especially during the coronavirus pandemic [3]. This adaptive response is linked to the microbes' ability to adapt and survive in the most diverse conditions, often in the form of biofilms.

Biofilms are colonies of microorganisms enclosed in extracellular polymeric substances (EPSs) attached to a surface [4]. Normally, the reversible attachment of planktonic (free-floating) bacteria on a substrate becomes irreversible in the presence of favorable conditions.

At first, cells proliferate and aggregate to form microcolonies, and then they create robust biofilms that are more resistant to antibiotic and antiseptic treatments [5]. The surrounding EPS physically protects these microorganisms in hostile environments, upregulating and exchanging genes responsible for producing antimicrobial resistance. To date, strategies that can effectively prevent bacterial adhesion to avoid the development of biofilms are highly demanded.

A promising approach to prevent the microbial colonization of surfaces turned out to be the use of micro- and nano-topographies, without involving the release of any biocidal agent to which pathogenic bacteria can develop resistance after a prolonged exposure [6,7]. The proposed killing mechanism for these antibacterial micro- and nano-tools has been depicted as a physical mechano-bactericidal action between the bacterial cell walls and the micro-/nano-structured surfaces [8]. Most of the models developed to figure out the dynamic networking between microorganisms and nanopatterned substrates have highlighted a bactericidal process that, depending on the shape of these nano-features, takes place via the stretching or cutting/piercing of the bacterial cell membrane [6,9–13]. In particular, nanopillar arrays have revealed their capability to induce bacterial membrane stretching [14,15], while sharp nano-edges have been reported to be responsible for cell wall damage via punctuations [16–19]. For both these nano-engineered substrates, it was observed that the mechano-bactericidal efficiency is strongly affected by their geometric nano-features (i.e., aspect ratio, spacing, and curvature radius) [20–24], thus suggesting that the fine-tuning of these characteristics at the nanoscale represents a valuable approach to modulate their antibacterial activity.

Among the most effective antimicrobial nanomaterials, carbon nanotubes (CNTs) have been extensively investigated, demonstrating their strong bactericidal properties toward both planktonic (free-floating bacteria) and biofilm (bacterial community) infections [25–27]. Most of the studies on the antibacterial properties of CNTs relate to their randomly oriented configuration and, in particular, to CNT-based suspensions. Despite their ascertained bacteria-killing effects [28–31], the use of CNTs dispersed in media still exhibits limitations, including the tendency to aggregate if not properly functionalized, which can reduce their antibacterial performances [32]. More critically, in the case of floating CNTs the results related to their cytotoxicity are conflicting, because they spread from negligible cellular reactions to severe toxic effects influenced by CNT length, diameter, concentration, and chemical functionalization [33–35]. However, when CNTs were strongly anchored on substrates, cytotoxicity consequences were not highlighted [36–38]. Notably, in order to tailor the antibacterial capacity of these carbon nanostructures, it is crucial to shape the spatial arrangement up to the sub-micrometric domain. In this regard, while CNTs dispersed in liquid media are difficult to control, vertically aligned carbon nanotubes (VA-CNTs), also known as CNT forests, can offer a tunable antibacterial platform thanks to the possibility to direct the tubes' alignment, diameter, length, and density via both in and ex situ processes [39,40]. The catalytic chemical vapor deposition (CVD) technique is the most widely exploited process for the synthesis of VA-CNTs [41]. Such an approach allows, in the presence of a carbon precursor (i.e., hydrocarbon source gas), the growth of highly oriented CNTs on solid substrates covered by a nanostructured catalytic element (i.e., Fe, Co, and Ni nanoparticles). In CVD synthesis, both catalyst characteristics (i.e., type, size, and density) and process parameters (i.e., growth temperature, reaction pressure and time, and gas composition and flow rate) dictate tube morphology and structural properties [42,43]. At the onset of CVD growth, straight and curved tubes are formed at the same macroscopic rate due to the interaction between fast- and slow-grown CNTs, thus leading to the self-arrangement of tubes in an entangled and randomly oriented configuration, known as the "crust layer" [44]. After the formation of such an intricate network of CNTs, the tubes continue to grow perpendicularly to the underlying substrate due to van der Waals interactions between them [45,46], displacing the crust on top of the forest [40].

The possibility of finely shaping this CNT-based crust, without damaging the microstructural integrity of the underlying VA-CNT forest, is crucial from the perspective of engineering the antibacterial activity of CNTs. Various strategies have been proposed to achieve this goal, including laser ablation [47], liquid-phase oxidation cutting, and electron beam and focused ion beam (FIB) processes [48]. However, these techniques can alter CNTs' features and alignment [49]. Alternatively, as in the case of FIB, a high level of precision in modifying the tube morphology can be achieved, but at the same time, undesired by-products and carbon redeposition are formed, and, in addition, long manufacturing times are required [50]. Conversely, plasma treatments have largely demonstrated to be capable of tailoring the morphology of CNTs in a controlled and time-efficient manner [40,51,52].

Herein, we firstly demonstrate that uniform, highly aligned, and densely packed CNTs can be successfully synthesized on SiO_2/Si substrates via a rapid (~15 min), cost-effective, and versatile synthesis method developed in a customized CVD system. The morphological (i.e., vertical alignment, density, and uniformity) and topographical (i.e., roughness, diameters, and height profiles) features of the as-grown highly oriented carbon nanostructures are assessed via field-emission scanning electron and atomic force microscopies (FE-SEM and AFM), while their surface composition is studied via X-ray photoelectron spectroscopy (XPS). Afterwards, the ability to tailor the surface morphology of VA-CNTs by means of plasma etching processes is exploited to systematically investigate the antimicrobial properties of different CNT-based substrates, with properly designed surfaces, against both Gram-positive (*Staphylococcus aureus*) and Gram-negative (*Pseudomonas aeruginosa*) bacteria.

2. Materials and Methods

2.1. CVD Synthesis of VA-CNTs

Vertically aligned carbon nanotubes were grown at the INFN CVD facility in Sapienza University of Rome by employing a customized thermal CVD reactor with a base pressure in the low 10^{-7} mbar range. This CVD facility has been developed for various applications, including the development of a novel dark matter detector [53–55]. Silicon p-type/Boron-doped < 100 > SiO_2/Si wafers, here adopted as growth substrates, were firstly cleaved into 40 mm × 20 mm chips and, subsequently, cleaned via the Radio Corporation of America (RCA) method. Electron beam (E-beam) evaporation was exploited for the deposition of a thin (3 nm in thickness) catalyst layer of iron over the Si-based substrates, which were then mounted on a heating element inside a high-vacuum reaction chamber and annealed at 720 °C in a H_2 atmosphere for 4 min. The purpose of such thermal treatment is twofold: firstly, to reduce iron oxides possibly developed on the surface of the Fe/SiO_2/Si substrate because of the exposure to the atmospheric air occurring when the sample is transferred from the E-beam evaporator to the CVD system and, secondly, to trigger the de-wetting of the catalyst layer and the nucleation of iron-based nanoparticles working as a template for subsequent CNT growth. After the annealing treatment, the reaction temperature was increased to 740 °C, and acetylene (carbon precursor) was fluxed inside the CVD chamber at a 300 sccm flow rate, without any carrier gas, up to a partial pressure of about 50 mbar. The growth time, intended as the time of interaction between the iron nanoparticles and the carbon source, was limited to 10 min. The optimization of the process parameters was based on previous studies related to the synthesis of VA-CNTs on different substrates [36–38,43]. Subsequently, the sample temperature was decreased to room temperature under the base pressure of the CVD system.

2.2. Plasma Etching Treatment

The as-grown VA-CNTs were subjected to O_2 and Ar/O_2 plasma treatments in a Plasmalab 80 plus reactive ion etching system from Plasmalab Technology (Everett, WA, USA). The etching studies were stimulated by a previous study [40], which first showed the possibility to remove the crust layer from CNT forests by means of Ar/O_2 plasma treatments. Here, we investigated different plasma etching conditions to tailor the crust layer by maintaining the typical high verticality of our VA-CNTs. CNT forests were

subjected to plasma etching with different RF powers (from 33 to 100 W), different Ar (from 0 to 52 sccm) and O_2 (from 2 to 195 sccm) flow rates, different residual pressures (from 1 to 200 mTorr), and different etching times (from 1 to 5 min) (Table S1). The effect of the plasma treatment on the VA-CNTs' morphology was evaluated by means of SEM, AFM, and XPS characterizations, and two different optimal etching conditions were finally selected: one with a combination of Ar and O_2 gas etching (10 sccm of Ar, 2 sccm of O_2, 35 W RF power, 200 mTorr residual pressure, 5 min of total etching time) and one with only O_2 gas etching (66 sccm of O_2, 100 W RF power, 40 mTorr residual pressure, 1 min of total etching time). The effects of these two conditions on the CNT morphology, roughness, surface composition, and antibacterial properties are reported below.

2.3. Characterization of VA-CNTs

FE-SEM imaging was conducted on the CNT forests, before and after the plasma etching processes, by collecting secondary electrons on a Zeiss Auriga SEM (Jena, Germany) operating at an accelerating voltage of 5 kV. Topographic measurements were performed with a Park Systems NX10 AFM (Suwon, Republic of Korea) in tapping mode, in air, by using a Nanosensors PPP-NCHR AFM tip (Neuchatel, Switzerland) and by collecting micrographs of 512 × 512 pixels at a cantilever speed of about 0.1 Hz. The surface composition of the VA-CNTs was investigated via an XPS analysis. An Omicron XM1000 monochromatized Al K_α X-ray source (Uppsala, Sweden) and a hemispherical electron analyzer (66 mm radius) equipped with a position-sensitive detector for parallel acquisition were employed. The energy of the X-rays was 1486.7 eV, and the total energy resolution was 520 meV. The C 1s spectra were fitted with Voigt profiles in order to take into account the experimental resolution and the intrinsic line width. The binding energy scale was calibrated with a clean sample of highly oriented pyrolytic graphite (HOPG) by setting the binding energy of the C1s core level to 284.5 eV [56].

2.4. Bacteria Growth Conditions and Cell Viability Test

The bacterial *Staphylococcus aureus* ATCC 25923 and *Pseudomonas aeruginosa* ATCC 15692 strains used in this study were grown in Luria–Bertani (LB) broth at 37 °C overnight under shaking. For cell viability tests, treated or untreated specimens, after 30 min of UV sterilization, were drop-casted with 15 µL of a bacterial suspension (1×10^8 cell/mL). Cells were recovered after 30 min, 4 h, and 24 h of incubation at 25 °C by submerging the substrates in a sterile tube with 2 mL of sterile H_2O_{dd} and shaking for 2 min. The extent of bacterial survival was assessed using the colony count method (Colony Forming Unit, CFU) by spreading the diluted samples (1×10^{-2} and 1×10^{-3} cell/mL) onto LB agar plates incubated at 37 °C overnight. The SiO_2/Si wafer samples w/o CNTs were used as a reference (untreated). The experiments were repeated three times, with three replicates for each treatment.

2.5. Biofilm Formation

For a biofilm production assay, an amount of 1×10^7 cells/mL of *S. aureus* or *P. aeruginosa* was inoculated in 3 mL of LB on a 35 mm Petri plate, in which different types of CNT samples (1 cm × 1 cm) were separately submerged. The plates were then incubated for 24 h at 37 °C. As a control, the bacterial strains were inoculated on plates where SiO_2/Si substrates (untreated samples) were soaked. After treatment, the cultures were gently removed, and the specimens were washed twice with sterile water and fixed for an SEM analysis.

2.6. Bacteria SEM Analysis

The investigated bacteria were fixed on the Si substrates, covered or not with CNTs, with 2% glutaraldehyde in sterile ultrapure H_2O for 1 h at room temperature in the dark. After 2 washes in sterile ultrapure H_2O (15 µL each), the samples were then dehydrated with sequential treatment with 30, 50, 70, 80, 90, and 96% ethanol for 5 min each. An

SEM microscopy of cells, interfaced or not with CNTs, was performed with a Zeiss Sigma 300 field-emission gun (Carl Zeiss S.p.a., Milano, Italy) operating at an accelerating voltage of 0.3 kV.

2.7. Reactive Oxygen Species Evaluation

For reactive oxygen species (ROS), treated or untreated specimens, after 30 min of UV sterilization, were drop-casted with 90 µL of a bacterial suspension (1×10^9 cell/mL). Cells were recovered after 2 h of incubation at 25 °C by submerging the substrates in a sterile tube with 1 mL of sterile H_2O_{dd} and shaking for 2 min.

Then, 100 µL aliquots from each sample were transferred into wells of a 96-well microtiter plate containing 100 µL of a 50 µM 2′,7′-dichlorofluorescein diacetate H_2DCFDA fluorescent probe (Sigma-Aldrich, Milan, Italy). Fluorescent signals were read immediately and after 60 min by using a microplate reader at excitation/emission wavelengths of 485 and 520 nm. The initial readings were subtracted from the final readings, and the mean fluorescence was calculated from the triplicate. The results are expressed as the ROS levels relative to those of the untreated specimens (UT) and are the mean of three independent experiments.

3. Results

An SEM analysis was conducted on the VA-CNTs, before and after the plasma etching treatments, to assess the impact of these post-growth processes on the tubes' morphology, alignment, and microstructural integrity. The optimization of the plasma etching parameters led to the identification of three main VA-CNT-based configurations, namely, light, modest, and aggressive etching (Figure S1), as suggested in [40], and here, they are indicated as as-grown, O_2-etched, and Ar/O_2-etched CNTs, respectively. A side-view SEM micrograph (Figure 1A) of the as-grown CNT forests revealed the presence of highly aligned and packed nanotubes, homogeneously covering the Si substrate, while, from the top view (Figure 1B, a higher magnification in the top-right inset), the CNTs appear with no preferential orientation. Such a uniform layer of randomly oriented CNTs, the "crust layer" formed during the early stages of the growth process [57], switches to a more spiky CNT arrangement after the O_2 plasma etching treatment (Figure 1D).

The sharper nanotube array, also shown at a higher SEM magnification (Figure 1D, in the top right indicated with an asterisk), does not involve a perturbation of the vertical alignment of the underlying CNTs (Figure 1C). Additionally, the CNTs were exposed to the Ar/O_2 plasma etching in order to increase their active surface by exploiting the combination of ion bombardment and the chemical reaction provided by the Ar and O_2 plasma etching, respectively [58,59]. In the side-view SEM image reported in Figure 1E, it is possible to appreciate that the configuration of the CNT forests totally changes with respect to that of the as-grown and O_2-plasma-treated CNTs. Indeed, the Ar/O_2 plasma etching causes a microstructural modification of the CNTs, leading them to arrange into micro-pillar arrays uniformly distributed over the Si substrate. The top-view SEM image (Figure 1F) shows a less rough topography when compared to both the as-grown (Figure 1B) and O_2-plasma-etched (Figure 1D) forests.

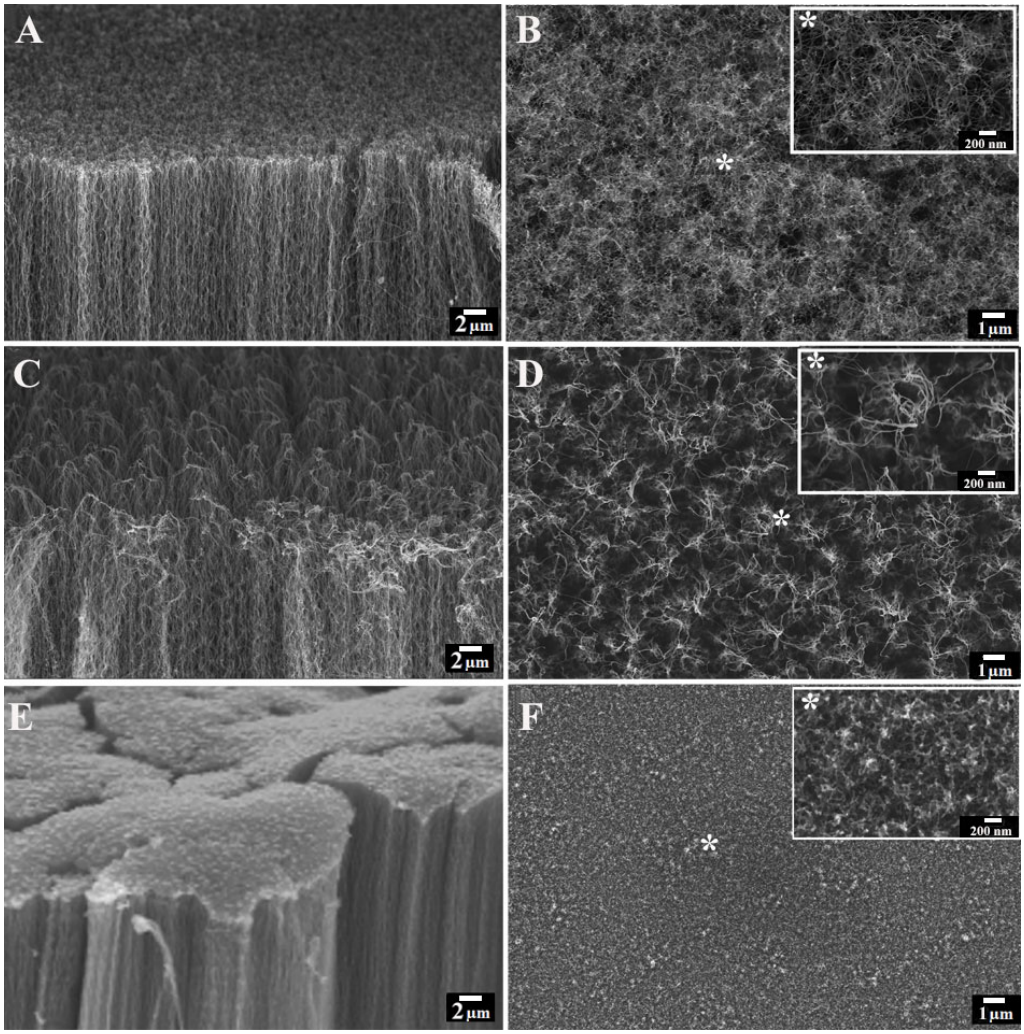

Figure 1. (**A**,**C**,**E**) Side- and (**B**,**D**,**F**) top-view SEM images of as-grown (**top**), O_2- (**middle**), and Ar/O_2-plasma-etched (**bottom**) VA-CNTs. Scale bar of star-signed inserts, showing top-view SEM images acquired at increased magnification of as-grown (**B**), O_2- (**D**), and Ar/O_2-(**F**) plasma-etched VA-CNTs: 200 nm.

The effect of the plasma etching on the CNTs' surface roughness, modified or not via plasma etching processes, was investigated via AFM to obtain a quantitative indication of the morphological variations that emerged from the SEM analysis. In particular, the RMS of the surface profile, as measured using AFM, was taken as an estimator of the surface roughness. Figure 2A shows the typical 3D topography of the as-grown CNTs exhibiting a surface roughness of 141.2 nm. Such an entangled fractal-like structure of nanotubes, deriving from their randomly oriented terminal part, was further pointed out via the SEM examination (Figure 2D). After the O_2 plasma etching treatment, a slight increase in terms of roughness (187.4 nm) was observed (Figure 2B), possibly ascribed to the formation of CNT aggregates assuming a configuration sharper than that highlighted in the top-view SEM micrograph reported in Figure 2E. However, after carrying out the Ar/O_2 plasma etching, a significant reduction in the top surface roughness (41.2 nm) was measured via AFM (Figure 2C), suggesting the potential removal of the crust layer, also identified in the SEM analysis (Figure 2F).

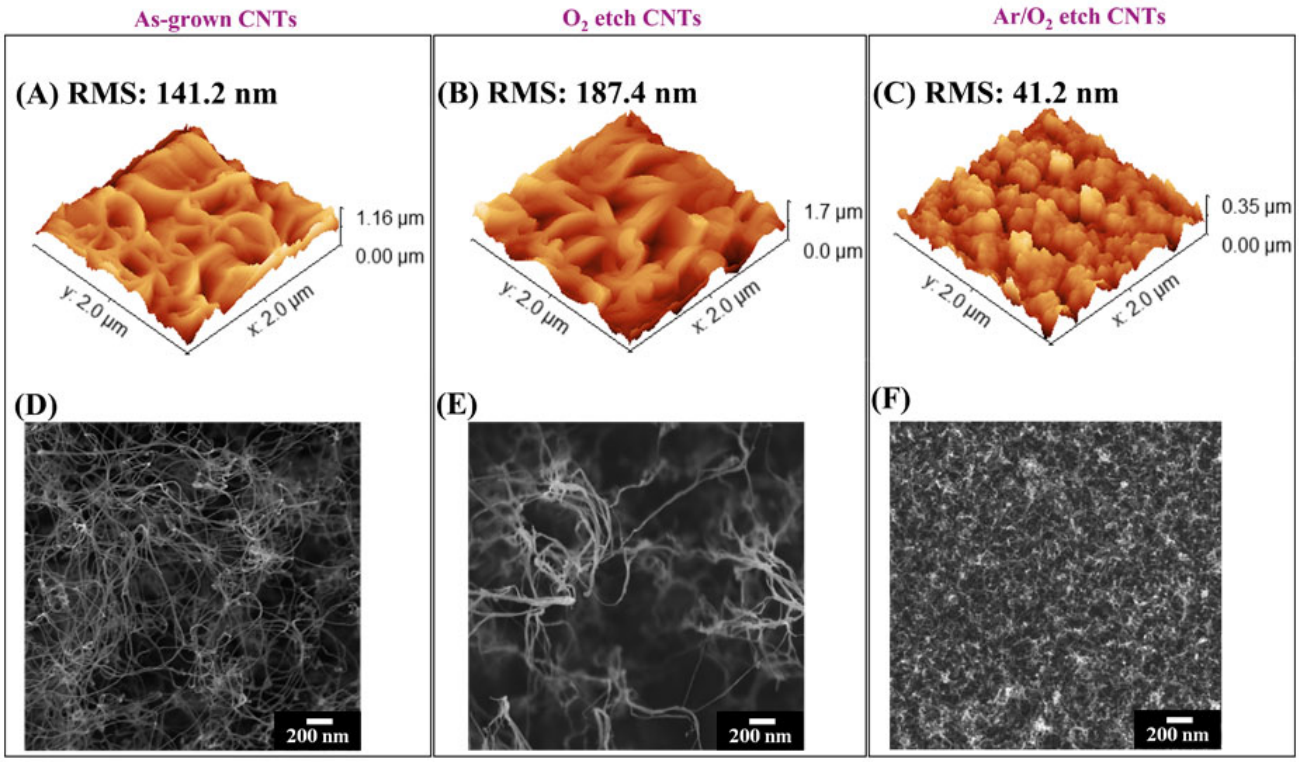

Figure 2. (**A**–**C**) AFM and (**D**–**F**) SEM images of VA-CNTs top surface for (**A**,**D**) as-grown, (**B**,**E**) O_2-, and (**C**,**F**) Ar/O_2-plasma-etched. Scale bar: 200 nm. In the top panels, the RMS of the top surface profile is reported.

To further investigate the surface chemical reaction occurring between the CNT forests and O_2 or Ar/O_2 etching gas, XPS characterization was performed. The XPS survey spectra, regardless of the plasma etching treatment, revealed the presence of two main elements: carbon (C1s) and oxygen (O1s) (Figure 3A). The C1s core level of the as-grown VA-CNTs (Figure 3B) pointed out the most intense peak (77%) at 284.3 eV assigned to sp^2-hybridized carbon atoms, along with a smaller component (6%) at 284.8 eV associated with the sp^3-like configuration and intrinsically related to CNT defects [60,61]. Additionally, together with the typical broad peak at 290.8 eV due to the π-plasmon, residual oxygen contamination (5%) was measured. After the O_2 and Ar/O_2 plasma etching (Figure 3C,D), only minor changes in the C1s core level spectra were detected: in both cases, the most intense peak was associated with sp^2-hybridized carbon (80% and 91%, respectively). The sp^3-like configuration was higher for the sample plasma-etched with O_2 (9%) than for the sample plasma-etched with Ar/O_2 (3%). Finally, the residual oxygen contamination was 5% and 1%, respectively, for the two plasma treatments.

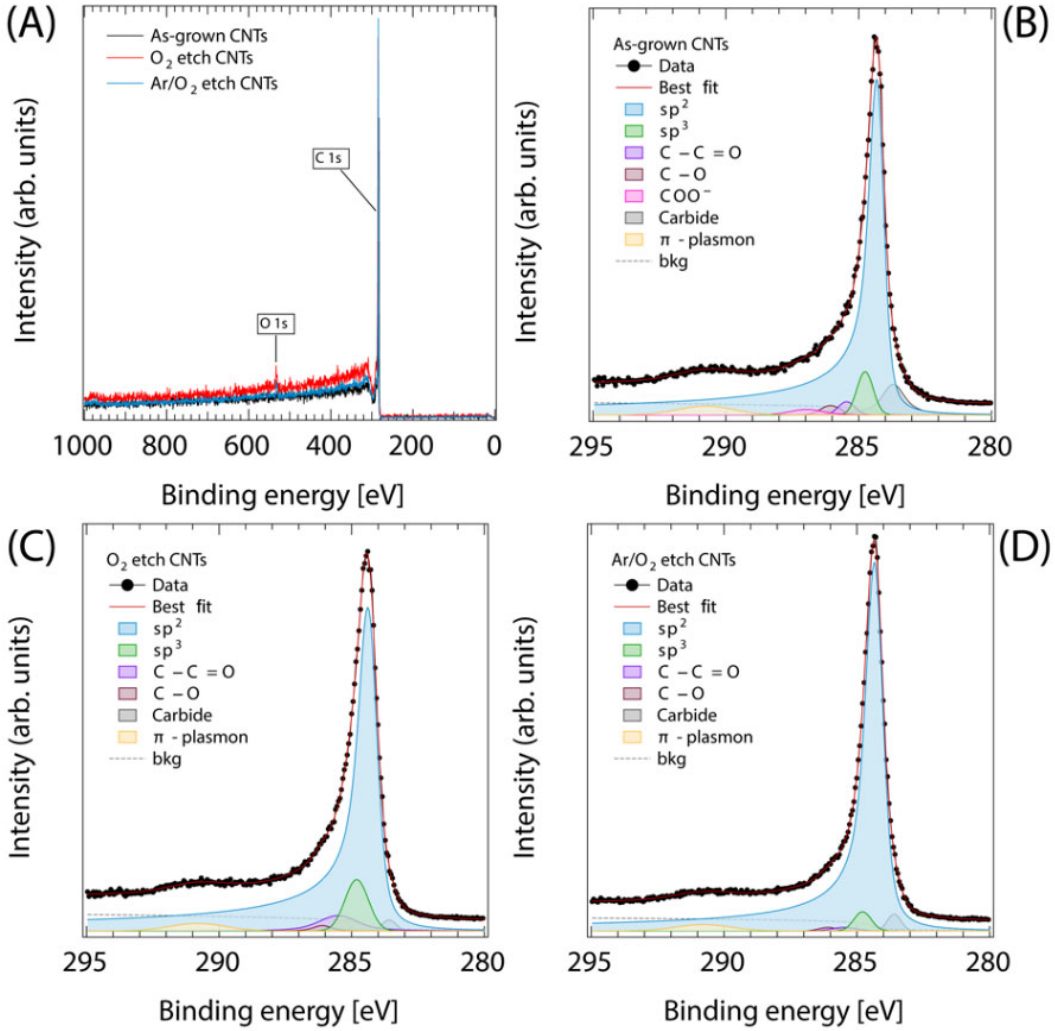

Figure 3. XPS survey (**A**) and C 1s of as-grown (**B**), O_2- (**C**), and Ar/O_2-plasma-etched (**D**) VA-CNTs.

As a representative of Gram-positive bacteria, *S. aureus* survival was evaluated by performing a CFU counting analysis after incubation with different CNT specimens. After only 30 min of treatment, a significant reduction of 97% in cell viability was observed in the presence of the Ar/O_2-etched CNTs with respect to that of the untreated cells. In the case of the as-grown and O_2-treated CNTs, notable viability reductions of about 90% and 70%, respectively, were highlighted after 4 h of treatment (Figure 4A). The interaction between the bacteria and the nanostructures was investigated through an FE-SEM analysis: the bacterial cell wall showed mechanical damages caused by direct contact with the nanotubes, which formed a network around the bacterium body, triggering cellular collapse (Figure 4B,C). This network became denser in the case of the Ar/O_2-treated CNTs, suggesting that the higher mortality observed in the cell viability tests could be due to the strong interactions with these nanostructures (Figure 4D). When testing the Gram-negative *P. aeruginosa*, similar behavior was observed. In particular, an almost total reduction (100%) of viability was observed after only 30 min of treatment with the Ar/O_2-etched CNTs (Figure 5A). When the cells were treated with the as-grown or O_2-treated CNTs, a reduction of 80% was detected after 4 h of treatment, and it reached 99.99% after 24 h. Moreover, in this case, through the FE-SEM analysis, it seems clear that cellular activity is extinguished by the nanotubes, which skewer or smother the bacterial cells (Figure 5B–D).

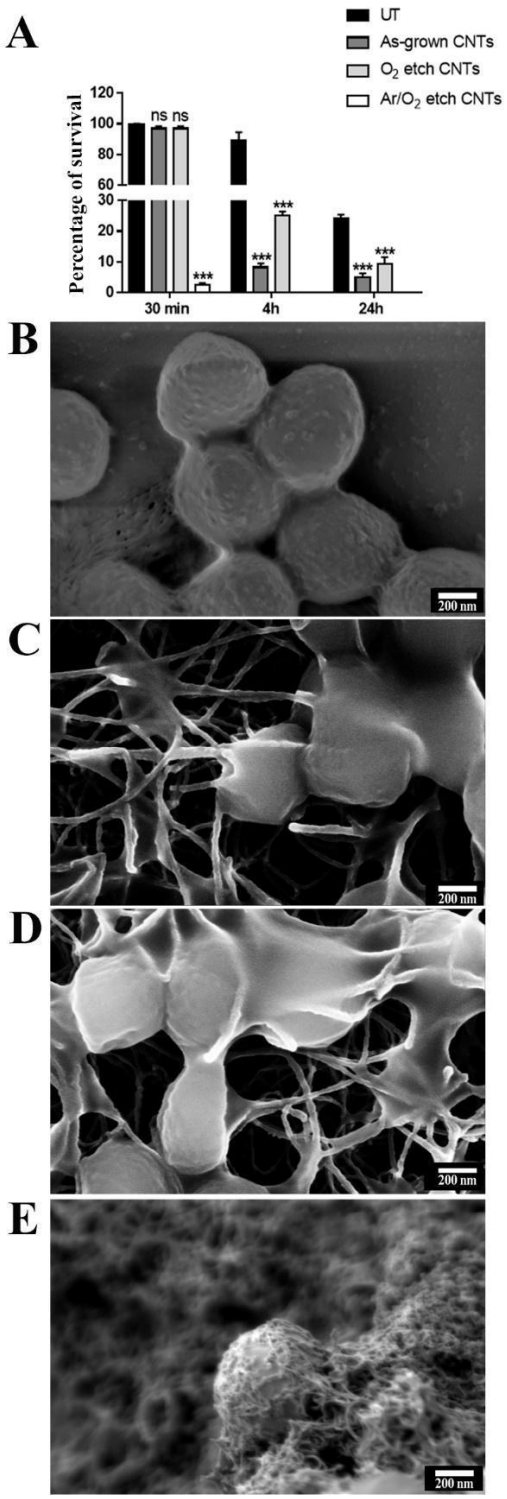

Figure 4. Antibacterial activity of VA-CNTs against *S. aureus*. (**A**) CFU percentage of *S. aureus* after 30 min, 4 h, and 24 h of incubation on Si substrates modified with CNTs. Bars represent the mean of three independent experiments. To assess statistical analysis, a one-way ANOVA analysis with the Bonferroni post-test was used; *** $p < 0.001$ with respect to untreated controls (UT); ns: not significant. The experiment was performed in triplicate for each treatment. SEM micrograph of (**B**) *S. aureus* bacteria incubated on Si substrate without carbon nanostructures in comparison with (**C**) as-grown, (**D**) O_2, and (**E**) Ar/O_2. Scale bar: 200 nm.

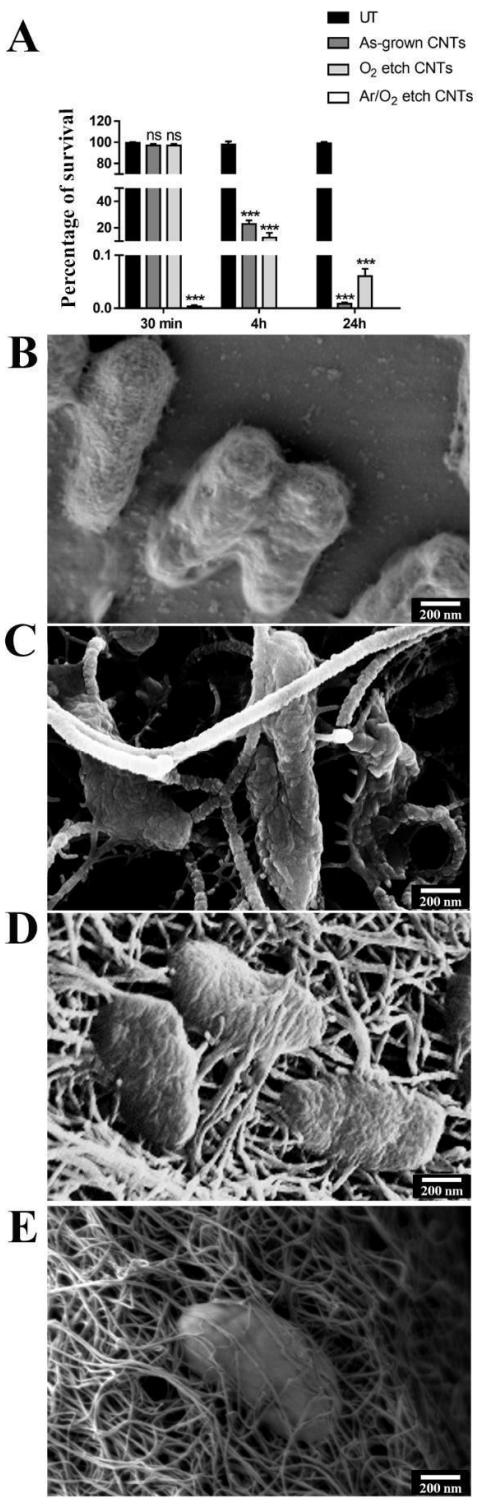

Figure 5. Antibacterial activity of VA-CNTs against *P. aeruginosa.* (**A**) Cell recovery by CFU counting of *P. aeruginosa* cells after 30 min, 4 h, and 24 h of incubation on Si substrates modified or not with different CNTs. Bars represent the mean of three independent experiments. To assess statistical analysis, a one-way ANOVA analysis with the Bonferroni post-test was used; *** $p < 0.001$ with respect to untreated controls (UT); ns: not significant. The experiment was performed in triplicate for each treatment. SEM micrograph of (**B**) *P. aeruginosa* bacteria incubated on Si substrates without carbon nanostructures in comparison with cells treated with (**C**) as-grown, (**D**) O_2-, and (**E**) Ar/O_2-plasma-etched VA-CNTs. Scale bar: 200 nm.

In the environment, microorganisms exist in the form of biofilms, made up of a group of cells that produce an extracellular matrix, allowing the bacterial population to resist adverse abiotic conditions [62]. For this reason, different CNT specimens were tested on cells' ability to produce biofilms (Figure 6). The results confirm the mechanical damage triggered by CNTs: the untreated cells were intact, showing their characteristic shape (round and rod-shaped morphology for *S. aureus* and *P. aeruginosa*, respectively). Conversely, in the treated cells, the bacterial surface showed mechanical injuries caused by direct contact with the CNTs, which adhered to the cell wall, causing its breakdown. After the incubation of the cells with the Ar/O_2-etched CNTs, interestingly, it was also possible to notice a strong reduction in the cell number in the observation field as compared to that in the untreated samples.

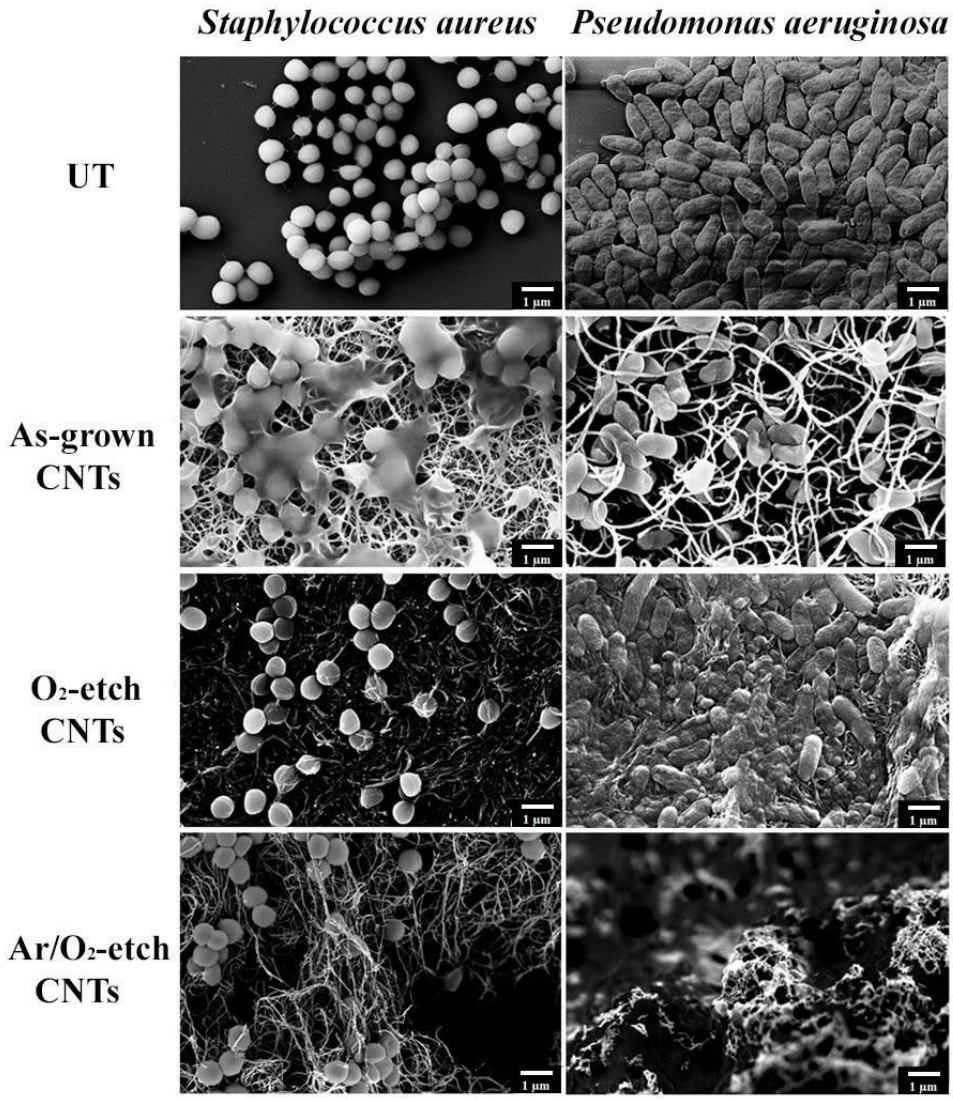

Figure 6. Antibiofilm activity of VA-CNTs against *S. aureus* and *P. aeruginosa*. FE-SEM micrographs of biofilm produced by Gram-positive or Gram-negative bacteria after 24 h incubation on Si substrates modified or not with different CNTs. Untreated (UT) samples were used as control. Bar, 1 µm.

To investigate the mechanisms of action of the different types of CNTs, bacterial oxidative stress was evaluated through a ROS accumulation analysis. Interestingly, the treatment of *S. aureus* with the VA-CNTs induced ROS production levels reaching 30% and 60% after incubation with the as-grown and Ar/O_2-etched CNTs, respectively (Figure 7A). However, the O_2-etched CNTs did not induce variations in ROS levels. In the case of

P. aeruginosa, all VA-CNTs could generate high levels of ROS, with a fraction of positive cells ranging from 20 to 50% (Figure 7B). In general, the Ar/O_2-etched CNTs resulted in the highest oxidative potential.

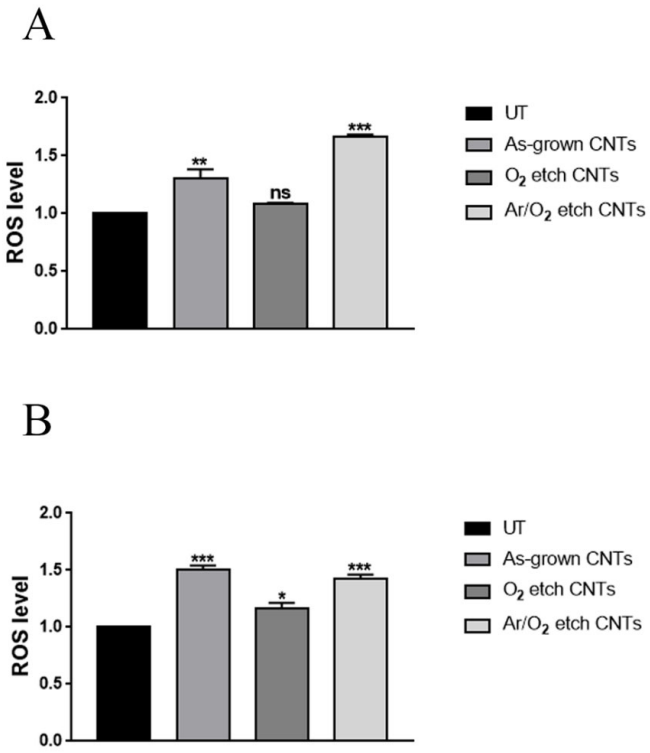

Figure 7. ROS production of (**A**) *S. aureus* and (**B**) *P. aeruginosa* after 2 h incubation on Si substrates modified or not with different CNTs. Untreated (UT) samples were used as control. Bars represent the mean of three independent experiments (* $p < 0.05$; ** $p < 0.01$; *** $p < 0.001$; ns: not significant).

4. Discussion

In this work, the antibacterial activity of CVD-grown VA-CNTs, modified or not with different plasma etching treatments, was tested. The CNTs were synthesized through a customized thermal CVD chamber enabling rapid (~15 min), cost-effective, and reproducible VA-CNT growth on a whole wafer (2 inch) or on different samples simultaneously. The resulting CNTs were multiwalled carbon nanotubes with diameters ranging between 15 and 25 nm and lengths up to 200 μm, as corroborated by SEM and TEM analyses performed on similar structures synthesized with the same procedure [36–38,43]. Various studies, aiming to evaluate the morphology and the degree of alignment of CNT forests through post-processing micrograph analyses or X-ray scattering techniques, have highlighted that these carbon nanostructures are not vertically aligned over their entire length [63–66]. In particular, a non-aligned crust layer, composed of randomly oriented carbon nanotubes, was observed over the top surface of the VA-CNT forests. The ability of VA-CNTs to modulate bacterial survival is strongly related to the micro- and nano-arrangements of the tubes along their whole length, from the base to the topside. In this direction, we designed experiments related to the modulation of CNTs' nanomorphology, with the final aim of exposing the sharp tips of the CNTs, considered the nano-features mostly responsible for bacterial wall damage via punctuations [16]. Therefore, since one of the most efficient strategies to tune CNTs' morphology, without altering their verticality, has turned out to be plasma etching, we investigated the impact of different plasma etching conditions firstly on the tube morphology and topography, via electron and atomic force microscopies, and then on the CNTs' surface composition by means of XPS characterization. Both the SEM and AFM analyses revealed the formation of spiky CNT bundles after O_2 plasma etching with an enhanced top-surface roughness when compared to that of the as-grown counterpart.

However, the combination of Ar and O_2 as an etching gas for the treatment gave rise to a less rough VA-CNT surface, thus suggesting the removal of the crust layer as proposed in a previous work [40]. At the same time, the surface composition characterized via the XPS technique revealed a dominant component related to sp^2-hybridized carbon for the three varieties of the CNT samples. Additionally, a small amount of sp^3-hybridized carbon was always present, and, in the case of the O_2-plasma-etched CNTs, it was slightly greater, probably due to the formation of spiky CNT bundles [40,60,61].

Carbon-based nanomaterials have unequivocally demonstrated their ability to kill bacteria [67,68]. Among them, CNTs, especially when dispersed in liquid media, have attracted increased attention as antimicrobial nanotools whose efficiency is highly affected by their purity, size distribution, dispersion state, and media [69]. VA-CNTs are, here, proposed as alternative antibacterial platforms by which it is possible to overcome the main issues related to CNT suspensions and, simultaneously, modulate the survival rate of microorganisms with improved effectiveness and a reduced interaction time. Indeed, different from what was observed previously [16] in the case of CNT suspensions, where antimicrobial effects were visible only after 24 h of treatment, here, a higher bactericidal action of the as-grown or O_2-etched VA-CNTs was measured after 4 h of treatment and after 30 min in the case of the Ar/O_2 CNT treatment. An FE-SEM analysis demonstrated that the CNT network observed around the bacterium body caused mechanical injuries to cell walls. This network became denser in the case of the Ar/O_2-modified CNTs, suggesting that the higher mortality observed in the cell viability tests could be due to the strong interactions with these nanostructures. These observations were most prominent with the Gram-negative *P. aeruginosa*, which possesses thin peptidoglycan layers of about five nm [70]. Since the mechanical damage could be due to interactions with external bacterial structures, the reduced susceptibility of *S. aureus* to VA-CNT deformation might partially be clarified by the increased peptidoglycan thickness, providing an increased rigidity and a higher turgor pressure. Overall, our observations highlight that Gram-negative *P. aeruginosa* was more sensitive than the Gram-positive *S. aureus* strains against the VA-CNTs tested. This behavior has also been observed in antimicrobial tests with nanopillar nanomaterials [70] and, in particular, with CVD-grown VA-CNTs modified or not with plasma etching treatments [71]. Nevertheless, they modified the thickness of CNT forests during growth and their surface chemistry with post-growth treatments by using O_2 or CF_4 as an etching gas in order to control the elastic energy stored in the nanotubes and their interaction with bacteria. Additionally, they achieved reduced bactericidal rates (99.3% for *P. aeruginosa* and 84.9% for *S. aureus*) compared with those reached in the present work (100% and 97% for *P. aeruginosa* and *S. aureus*, respectively), where O_2 or a combination of Ar and O_2 was exploited to modulate VA-CNTs' nanomorphology and, consequently, their antimicrobial power without altering their surface compositions. The mechanism of CNTs' toxicity is highly influenced by several factors, such as their diameter, length, electronic structure, and surface functional group [72]. In general, it has been reported that the antimicrobial activity could be affected by different mechanisms. The first phase includes physical contact between the CNTs and bacteria, following the bacterial membrane perturbation caused by this interaction (phase 2) [73]. The third phase is characterized by electronic structure-dependent bacterial oxidation and subsequent cell membrane damage and death [70]. The first parameter involved is the length of the nanotubes, which influences the interactions with the cell membrane of bacteria. Indeed, shorter tubes seem to exert superior bactericidal performance, increasing the interaction between the open ends of nanotubes and a microorganism [74]. Moreover, smaller diameters can also damage cell membranes, penetrating the interior of the cell and preventing cell proliferation. This induces cell lysis and kills the bacteria. The attachment of CNTs alters the structure, permeability, and proton motive force of the cell membrane. Several studies have shown that the contact of bacteria with CNTs causes cell morphology distortion, damage to cell membrane integrity, and the release of intracellular material [75–77]. Although these studies reported that the cytotoxicity of CNTs against bacteria is due to cell membrane

damage caused by direct contact, the antibacterial effect could be further related to the production of ROS in CNT-treated cells [78]. In general, ROS, including the superoxide anion ($O^{2\bullet-}$), hydrogen peroxide (H_2O_2), hydroxyl radical ($^\bullet OH$), and singlet oxygen ($^1O_2$), can be produced within the cell as an unavoidable consequence of bacterial metabolism or derived from the environment [79]. Highly active ROS, especially $^1O_2$, can directly cause oxidative damage to nucleic acids, proteins, lipids, and other external structures of bacteria, resulting in genotoxicity, protein dysfunction and membrane disruption, and finally bacteria death [80]. On these bases, the high antimicrobial power of the Ar/O_2-etched VA-CNTs seemed to be due to the synergistic effects of both mechanical injuries and high levels of ROS production. As reported in [73], these metallic nanotubes could induce oxidative stress by acting as a conductive bridge with the bacterial membrane. It has been reported that VA-CNTs demonstrate better field emission than randomly oriented CNTs [81]. Indeed, in the Ar/O_2-etched VA-CNTs, the crust on top of the forest was removed, allowing them to "short-circuit" the bacteria.

Thanks to their physical properties and morphologies, VA-CNTs are becoming the most attractive nanomaterials for biologically active surfaces. Furthermore, their surface characteristics can be altered through various post-treatment techniques, such as chemical modification and plasma processing. Compared to non-aligned structures, VA-CNT arrays are of specific interest due to their larger available surface area, higher packing density, and controllable microstructure. Finally, controlling the interactions between the surface of nanostructures and cellular organisms can have vital implications for a host of fields, such as in medicine, agrochemical industries, and pharmaceutics. These examples show the usefulness of nanostructures in bio-related applications.

5. Conclusions

This study proposes and demonstrates the possibility of designing highly antibacterial coatings with vertically aligned carbon nanotubes, produced by means of an easy, low-cost, and fast (~15 min) chemical vapor deposition process. Different plasma etching treatments were exploited to modulate, up to the sub-micrometric domain, the surface topography of VA-CNTs. Among the different types of developed VA-CNT-based substrates, we found that the combination of Ar and O_2 as an etching gas gave rise to the most efficient antibacterial power, with an almost complete reduction in bacterial viability after only 30 min of treatment. Additionally, this work sheds light on the mechanism responsible for this exceptional antimicrobial activity of CNT forests, pointing out that it occurs due to the mechanical interaction between the bacterial cell walls and the nanotube structures, which are capable of "skewering" or "smothering" the bacteria and, simultaneously, producing high levels of ROS, thus preventing the formation of microbial colonies. The synthesis process proposed here, involving the CVD growth of CNT forests followed by the subsequent tuning of their nanomorphology through plasma etching, is an effective, rapid (CVD synthesis and plasma etching time is around 20 min overall), and low-cost route for engineering antibacterial films for a wide range of applications, such as biomedical devices, filtering systems for hospitals, and solid–air/liquid interfaces in healthcare units where biofilms usually appear.

Supplementary Materials: The following supporting information can be downloaded at: https://www.mdpi.com/article/10.3390/nano13061081/s1, Table S1. Optimization of plasma treatment conditions. Figure S1. (A–I) Top view SEM micrographs of VA-CNTs modified with different plasma etching conditions showing the morphology of: (A) sample 1 in Table S1 where no significant morphological alterations occur and the crust layer seems to be still present over the surface of CNT mats (i.e., "light" etching), (B,C) samples identified as 2 and 3 in Table S1 in which the uniform layer of randomly oriented CNTs (i.e., crust layer) switches to a more spiky CNTs arrangement, categorized as "aggressive" etching, (D–H) samples 4–8, upon which significant morphological and structural alterations emerge, (I) sample 9 where the crust is removed and the structural integrity of CNT forests is maintained, identified as "modest" etching.

Author Contributions: Methodology, validation, visualization, writing—original draft preparation, E.S.; software, funding acquisition, project administration, writing—review and editing, G.C.; methodology, investigation, data curation, writing—review and editing, F.P.; formal analysis, supervision, resources, writing—review and editing, D.U.; methodology, validation, visualization, writing—review and editing, G.P.; methodology, validation, data curation, writing—review and editing, A.A.; methodology, validation, data curation, writing—review and editing, A.R.; conceptualization, methodology, writing—original draft, supervision, I.R. All authors have read and agreed to the published version of the manuscript.

Funding: This work was funded by Progetto Medio Ateneo 2020 of Sapienza University of Rome "Nanobio" RM120172B7FEC4B8 and in part by ATTRACT project funded by the EC under Grant Agreement 777222. Additional funding was provided by project 2020Y2JMP5 'ANDROMeDa' (CUP: I85F21004170005) funded by MUR.

Data Availability Statement: The data presented in this study are available on request from the corresponding author.

Acknowledgments: We thank G. De Bellis (CNIS, Center on Nanotechnology Applied to Engineering of Sapienza) for help in the analyses and comments on the SEM experiments. Ilaria Rago acknowledges support from the Amaldi Research Center funded by the MIUR program "Dipartimento di Eccellenza" (CUP:B81I18001170001).

Conflicts of Interest: The authors declare no conflict of interest. The funders had no role in the design of the study; in the collection, analyses, or interpretation of data; in the writing of the manuscript; or in the decision to publish the results.

References

1. Heuer, H.; Smalla, K. Horizontal gene transfer between bacteria. *Env. Biosaf. Res.* **2007**, *6*, 3–13. [CrossRef] [PubMed]
2. Ren, R.; Lim, C.; Li, S.; Wang, Y.; Song, J.; Lin, T.; Muir, B.W.; Hsu, H.; Shen, H. Recent Advances in the Development of Lipid-, Metal-, Carbon-, and Polymer-Based Nanomaterials for Antibacterial Applications. *Nanomaterials* **2022**, *12*, 3855. [CrossRef]
3. Lucien, M.A.B.; Canarie, M.F.; Kilgore, P.E.; Jean-Denis, G.; Fénélon, N.; Pierre, M.; Cerpa, M.; Joseph, G.A.; Maki, G.; Zervos, M.J.; et al. Antibiotics and antimicrobial resistance in the COVID-19 era: Perspective from resource-limited settings. *Int. J. Infect. Dis.* **2021**, *104*, 250–254. [CrossRef]
4. Deep, K.K.; Olivier, H. Death at the interface: Nanotechnology's challenging frontier against microbial surface colonization. *Front. Chem.* **2022**, *10*, 1003234.
5. Vadrucci, M.; De Bellis, G.; Mazzuca, C.; Mercuri, F.; Borgognoni, F.; Schifano, E.; Uccelletti, D.; Cicero, C. Effects of the Ionizing Radiation Disinfection Treatment on Historical Leather. *Front. Mater.* **2020**, *7*, 00021. [CrossRef]
6. Naskar, A.; Kim, K. Nanomaterials as Delivery Vehicles and Components of New Strategies to Combat Bacterial Infections: Advantages and Limitations. *Microorganisms* **2019**, *7*, 356. [CrossRef]
7. Linklater, D.P.; Baulin, V.A.; Juodkazis, S.; Crawford, R.J.; Stoodley, P.; Ivanova, E.P. Mechano-bactericidal actions of nanostructured surfaces. *Nat. Rev. Microbiol.* **2021**, *19*, 8–22. [CrossRef]
8. Anderl, J.N.; Franklin, M.J.; Stewart, P.S. Role of Antibiotic Penetration Limitation in Klebsiella Pneumoniae Biofilm Resistance to Ampicillin and Ciprofloxacin. *Antimicrob. Agents Chemother.* **2000**, *44*, 1818–1824. [CrossRef]
9. Linklater, D.P.; Juodkazis, S.; Rubanov, S.; Ivanova, E.P. Comment on "Bactericidal Effects of Natural Nanotopography of Dragonfly Wing on *Escherichia coli*". *ACS Appl. Mater. Interfaces* **2017**, *9*, 29387. [CrossRef]
10. Ishak, M.I.; Jenkins, J.; Kulkarni, S.; Keller, T.F.; Briscoe, W.H.; Nobbs, A.H.; Su, B. Insights into complex nanopillar-bacteria interactions: Roles of nanotopography and bacterial surface proteins. *J. Colloid Interface Sci.* **2021**, *604*, 91–103. [CrossRef]
11. Bandara, C.D.; Singh, S.; Afara, I.O.; Wolff, A.; Tesfamichael, T.; Ostrikov, K.; Oloyede, A. Bactericidal Effects of Natural Nanotopography of Dragonfly Wing on *Escherichia coli*. *ACS Appl. Mater. Interfaces* **2017**, *9*, 6746–6760. [CrossRef]
12. Watson, G.S.; Green, D.W.; Watson, J.A.; Zhou, Z.; Li, X.; Cheung, G.S.P.; Gellender, M. A simple model for binding and rupture of bacterial cells on nanopillar surfaces. *Adv. Mater. Interfaces* **2019**, *6*, 1801646. [CrossRef]
13. Ayazi, M.; Ebrahimi, N.G.; Nodoushan, E.J. Bacterial adhesion reduction on the surface with a simulated pattern: An insight into extrand model. *Int. J. Adhes. Adhes.* **2019**, *88*, 66–73. [CrossRef]
14. Li, X. Bactericidal mechanism of nanopatterned surfaces. *Phys. Chem. Chem. Phys.* **2016**, *18*, 1311–1316. [CrossRef]
15. Pogodin, S.; Hasan, J.; Baulin, V.A.; Webb, H.K.; Truong, V.K.; Nguyen, T.H.P.; Boshkovikj, V.; Fluke, C.J.; Watson, G.S.; Watson, J.A.; et al. Biophysical model of bacterial cell interactions with nanopatterned cicada wing surfaces. *Biophys. J.* **2013**, *104*, 835–840. [CrossRef]
16. Olivi, M.; Zanni, E.; De Bellis, G.; Talora, C.; Sarto, M.S.; Palleschi, C.; Flahaut, E.; Monthioux, M.; Rapino, S.; Uccelletti, D.; et al. Inhibition of microbial growth by carbon nanotube networks. *Nanoscale* **2013**, *5*, 9023. [CrossRef]

17. Pham, V.T.H.; Truong, V.K.; Quinn, M.D.J.; Notley, S.M.; Guo, Y.; Baulin, V.A.; Al Kobaisi, M. Graphene induces formation of pores that kill spherical and rod- shaped bacteria. *ACS Nano* **2015**, *9*, 8458–8467. [CrossRef]
18. Lu, X.; Feng, X.; Werber, J.R.; Chu, C.; Zucker, I.; Kim, J.; Osuji, C.O.; Elimelech, M. Enhanced antibacterial activity through the controlled alignment of graphene oxide nanosheets. *Proc. Natl Acad. Sci. USA* **2017**, *114*, E9793–E9801. [CrossRef]
19. Pandit, S.; Gaska, K.; Mokkapati, V.R.S.S.; Celauro, E.; Derouiche, A.; Forsberg, S.; Svensson, M.; Kádár, R.; Mijakovic, I. Precontrolled alignment of graphite nanoplatelets in polymeric composites prevents bacterial attachment. *Small* **2020**, *16*, 1904756. [CrossRef]
20. Linklater, D.P.; Ivanova, E.P. Nanostructured antibacterial surfaces—What can be achieved? *Nano Today* **2022**, *43*, 101404. [CrossRef]
21. Linklater, D.P.; Juodkazis, S.; Ivanova, E.P. Nanofabrication of mechano-bactericidal surfaces. *Nanoscale* **2017**, *9*, 16564–16585. [CrossRef]
22. Linklater, D.P.; Nguyen, H.K.D.; Bhadra, C.M.; Juodkazis, S.; Ivanova, E.P. Influence of nanoscale topology on bactericidal efficiency of black silicon surfaces. *Nanotechnology* **2017**, *28*, 245301. [CrossRef]
23. Bhadra, C.M.; Werner, M.; Baulin, V.A.; Truong, V.K.; Kobaisi, M.A.; Nguyen, S.H.; Balcytis, A.; Juodkazis, S.; Wang, J.Y.; Mainwaring, D.E.; et al. Subtle Variations in Surface Properties of Black Silicon Surfaces Influence the Degree of Bactericidal Efficiency. *Nano-Micro Lett.* **2018**, *10*, 36. [CrossRef]
24. Ivanova, E.P.; Hasan, J.; Webb, H.K.; Gervinskas, G.; Juodkazis, S.; Truong, V.K.; Lamb, R.N.; Baulin, V.A.; Watson, G.S.; Watson, J.A.; et al. Bactericidal Activity of Black Silicon. *Nat. Commun.* **2013**, *4*, 2838. [CrossRef]
25. Mocan, T.; Matea, C.T.; Pop, T.; Mosteanu, O.; Buzoianu, A.D.; Suciu, S.; Puia, C.; Zdrehus, C.; Iancu, C.; Mocan, L. Carbon nanotubes as anti-bacterial agents. *Cell. Mol. Life Sci.* **2017**, *74*, 3467–3479. [CrossRef]
26. Malek, I.; Schaber, C.F.; Heinlein, T.; Schneider, J.J.; Gorb, S.N.; Schmitz, R.A. Vertically aligned multi walled carbon nanotubes prevent biofilm formation of medically relevant bacteria. *J. Mater. Chem. B* **2016**, *4*, 5228–5235. [CrossRef]
27. Corletto, A.; Shapter, J.G. Nanoscale Patterning of Carbon Nanotubes: Techniques, Applications, and Future. *Adv. Sci.* **2021**, *8*, 2001778. [CrossRef]
28. Kang, S.; Herzberg, M.; Rodrigues, D.F.; Elimelech, M. Antibacterial Effects of Carbon Nanotubes: Size Does Matter! *Langmuir* **2008**, *24*, 6409–6413. [CrossRef]
29. Yang, C.; Mamouni, J.; Tang, Y.; Yang, L. Antimicrobial Activity of Single-Walled Carbon Nanotubes: Length Effect. *Langmuir* **2010**, *26*, 16013–16019. [CrossRef]
30. Chen, H.; Wang, B.; Gao, D.; Guan, M.; Zheng, L.; Ouyang, H.; Chai, Z.; Zhao, Y.; Feng, W. Broad-Spectrum Antibacterial Activity of Carbon Nanotubes to Human Gut Bacteria. *Small* **2013**, *9*, 2735–2746. [CrossRef]
31. Le, T.T.A.; McEvoy, J.; Khan, E. Mitigation of Bactericidal Effect of Carbon Nanotubes by Cell Entrapment. *Sci. Total Environ.* **2016**, *565*, 787–794. [CrossRef]
32. Kohls, A.; Ditty, M.M.; Dehghandehnavi, F.; Zheng, S.Y. Vertically Aligned Carbon Nanotubes as a Unique Material for Biomedical Applications. *ACS Appl. Mater. Interfaces* **2022**, *14*, 6287–6306. [CrossRef]
33. Allegri, M.; Perivoliotis, D.K.; Bianchi, M.G.; Chiu, M.; Pagliaro, A.; Koklioti, M.A.; Trompeta, A.A.; Bergamaschi, E.; Bussolati, O.; Charitidis, C.A. Toxicity determinants of multi-walled carbon nanotubes: The relationship between functionalization and agglomeration. *Toxicol. Rep.* **2016**, *19*, 230–243. [CrossRef]
34. Liu, Y.; Zhao, Y.; Sun, B.; Chen, C. Understanding the toxicity of carbon nanotubes. *Acc. Chem. Res.* **2013**, *46*, 702–713. [CrossRef]
35. Kobayashi, N.; Izumi, H.; Morimoto, Y. Review of toxicity studies of carbon nanotubes. *J. Occup. Health* **2017**, *59*, 394–407. [CrossRef]
36. Rago, I.; Rauti, R.; Bevilacqua, M.; Calaresu, I.; Pozzato, A.; Cibinel, M.; Dalmiglio, M.; Tavagnacco, C.; Goldoni, A.; Scaini, D. Carbon nanotubes, directly grown on supporting surfaces, improve neuronal activity in hippocampal neuronal networks. *Adv. Biosyst.* **2019**, *3*, 1800286. [CrossRef]
37. Pampaloni, N.P.; Rago, I.; Calaresu, I.; Cozzarini, L.; Casalis, L.; Goldoni, A.; Ballerini, L.; Scaini, D. Transparent carbon nanotubes promote the outgrowth of enthorino-dentate projections in lesioned organ slice cultures. *Dev. Neurobiol.* **2020**, *80*, 316–331. [CrossRef]
38. Ulloa, L.S.; Perissinotto, F.; Rago, I.; Goldoni, A.; Santoro, R.; Pesce, M.; Casalis, L.; Scaini, D. Carbon nanotubes substrates alleviate pro-calcific evolution in porcine valve interstitial cells. *Nanomaterials* **2021**, *11*, 2724. [CrossRef]
39. Goh, G.L.; Agarwala, S.; Yeong, W.Y. Directed and On-Demand Alignment of Carbon Nanotube: A Review toward 3D Printing of Electronics. *Adv. Mater. Interfaces* **2019**, *6*, 1801318. [CrossRef]
40. Seo, S.; Kim, S.; Yamamoto, S.; Cui, K.; Kodama, T.; Shiomi, J.; Inoue, T.; Chiashi, S.; Maruyama, S.; Hart, A.J. Tailoring the surface morphology of carbon nanotube forests by plasma etching: A parametric study. *Carbon* **2021**, *180*, 204–214. [CrossRef]
41. Schneider, J.J. Vertically Aligned Carbon Nanotubes as Platform for Biomimetically Inspired Mechanical Sensing, Bioactive Surfaces, and Electrical Cell Interfacing. *Adv. Biosys.* **2017**, *1*, 1700101. [CrossRef]
42. Sharma, P.; Pavelyev, V.; Kumar, S.; Mishra, P.; Islam, S.S.; Tripathi, N. Analysis on the synthesis of vertically aligned carbon nanotubes: Growth mechanism and techniques. *J. Mater. Sci. Mater. Electron.* **2020**, *31*, 4399–4443. [CrossRef]
43. Sarasini, F.; Tirillò, J.; Lilli, M.; Bracciale, M.P.; Vullum, P.E.; Berto, F.; De Bellis, G.; Tamburrano, A.; Cavoto, G.; Pandolfi, F.; et al. Highly aligned growth of carbon nanotube forests with in-situ catalyst generation: A route to multifunctional basalt fibres. *Compos. Part B Eng.* **2022**, *243*, 110136. [CrossRef]

44. Zhang, Q.; Zhou, W.; Qian, W.; Xiang, R.; Huang, J.; Wang, D.; Wei, F. Synchronous Growth of Vertically Aligned Carbon Nanotubes with Pristine Stress in the Heterogeneous Catalysis Process. *J. Phys. Chem. C* **2007**, *111*, 14638–14643. [CrossRef]
45. Xu, M.; Futaba, D.N.; Yumura, M.; Hata, K. Alignment control of carbon nanotube forest from random to nearly perfectly aligned by utilizing the crowding effect. *ACS Nano* **2012**, *6*, 5837–5844. [CrossRef]
46. Landois, P.; Pinault, M.; Rouzière, S.; Porterat, D.; Mocuta, C.; Elkaim, E.; Mayne-L'Hermite, M.; Launois, P. In situ time resolved wide angle X-ray diffraction study of nanotube carpet growth: Nature of catalyst particles and progressive nanotube alignment. *Carbon* **2015**, *87*, 246–256. [CrossRef]
47. Gbordzoe, S.; Yarmolenko, S.; Kanakaraj, S.; Haase, M.R.; Alvarez, N.T.; Borgemenke, R.; Adusei, P.K.; Shanov, V. Effects of laser cutting on the structural and mechanical properties of carbon nanotube assemblages. *Mater. Sci. Eng. B* **2017**, *223*, 143–152. [CrossRef]
48. Wu, X.; Yin, H.; Li, Q. Ablation and Patterning of Carbon Nanotube Film by Femtosecond Laser Irradiation. *Appl. Sci.* **2019**, *9*, 3045. [CrossRef]
49. De Volder, M.; Hart, A.J. Engineering hierarchical nanostructures by elastocapillary self-assembly. *Angew. Chem. Int. Ed.* **2013**, *52*, 2412–2425. [CrossRef]
50. Sears, K.; Skourtis, C.; Atkinson, K.; Finn, N.; Humphries, W. Focused ion beam milling of carbon nanotube yarns to study the relationship between structure and strength. *Carbon* **2010**, *48*, 4450–4456. [CrossRef]
51. Xu, M.; Du, F.; Ganguli, S.; Roy, A.; Dai, L. Carbon nanotube dry adhesives with temperature-enhanced adhesion over a large temperature range. *Nat. Commun.* **2016**, *7*, 13450. [CrossRef]
52. Hou, Z.; Cai, B.; Liu, H.; Xu, D. Ar, O_2, CHF3, and SF6 plasma treatments of screen-printed carbon nanotube films for electrode applications. *Carbon* **2008**, *46*, 405–413. [CrossRef]
53. Cavoto, G.; Luchetta, F.; Polosa, A.D. Sub-GeV dark matter detection with electron recoils in carbon nanotubes. *Phys. Lett. B* **2018**, *776*, 338–344. [CrossRef]
54. Capparelli, L.M.; Cavoto, G.; Mazzilli, D.; Polosa, A.D. Directional dark matter searches with carbon nanotubes. *Phys. Dark Universe* **2015**, *9*, 24–30. [CrossRef]
55. Cavoto, G.; Cirilllo, E.N.M.; Cocina, F.; Ferretti, J.; Polosa, A.D. WIMP detection and slow ion dynamics in carbon nanotube arrays. *Eur. Phys. J. C* **2016**, *76*, 76. [CrossRef]
56. Chen, X.; Wang, X.; Fang, D. A review on C1s XPS-spectra for some kinds of carbon materials. *Fuller. Nanotub. Carbon Nanostruct.* **2020**, *28*, 1048–1058. [CrossRef]
57. Zhang, L.; Li, Z.; Tan, Y.; Lolli, G.; Sakulchaicharoen, N.; Requejo, F.G.; Mun, B.S.; Resasco, D.E. Influence of a Top Crust of Entangled Nanotubes on the Structure of Vertically Aligned Forests of Single-Walled Carbon Nanotubes. *Chem. Mater.* **2006**, *18*, 5624–5629. [CrossRef]
58. He, B.; Yang, Y.; Yuen, M.F.; Chen, X.F.; Lee, C.S.; Zhang, W.J. Vertical nanostructure arrays by plasma etching for applications in biology, energy, and electronics. *Nano Today* **2013**, *8*, 265–289. [CrossRef]
59. Puliyalil, H.; Cvelbar, U. Selective plasma etching of polymeric substrates for advanced applications. *Nanomaterials* **2016**, *6*, 108. [CrossRef]
60. Kim, B.J.; Kim, J.P.; Park, J.S. Effects of Al interlayer coating and thermal treatment on electron emission characteristics of carbon nanotubes deposited by electrophoretic method. *Nanoscale Res. Lett.* **2014**, *9*, 236. [CrossRef]
61. Okpalugo, T.I.T.; Papakonstantinou, P.; Murphy, H.; McLaughlin, J.; Brown, N.M.D. High resolution XPS characterization of chemical functionalised MWCNTs and SWCNTs. *Carbon* **2005**, *43*, 153–161. [CrossRef]
62. Schifano, E.; Cavallini, D.; De Bellis, G.; Bracciale, M.P.; Felici, A.C.; Santarelli, M.L.; Sarto, M.S.; Uccelletti, D. Antibacterial Effect of Zinc Oxide-Based Nanomaterials on Environmental Biodeteriogens Affecting Historical Buildings. *Nanomaterials* **2020**, *10*, 335. [CrossRef]
63. Gao, Y.; Kodama, T.; Won, Y.; Dogbe, S.; Pan, L.; Goodson, K.E. Impact of nanotube density and alignment on the elastic modulus near the top and base surfaces of aligned multi-walled carbon nanotube films. *Carbon* **2012**, *50*, 3789–3798. [CrossRef]
64. Bedewy, M.; Meshot, E.R.; Guo, H.; Verploegen, E.A.; Lu, W.; Hart, A.J. Collective mechanism for the evolution and self-termination of vertically aligned carbon nanotube growth. *J. Phys. Chem. C* **2009**, *113*, 20576–20582. [CrossRef]
65. Wang, B.N.; Bennett, R.D.; Verploegen, E.; Hart, A.J.; Cohen, R.E. Quantitative characterization of the morphology of multiwall carbon nanotube films by small-angle x-ray scattering. *J. Phys. Chem. C* **2007**, *111*, 5859–5865. [CrossRef]
66. Malik, H.; Stephenson, K.; Bahr, D.; Field, D. Quantitative characterization of carbon nanotube turf topology by SEM analysis. *J. Mater. Sci.* **2011**, *46*, 3119–3126. [CrossRef]
67. Seifi, T.; Kamali, A.R. 3D-graphene nanosheets as efficient antibacterial agent. *Mater. Lett.* **2022**, *321*, 132406. [CrossRef]
68. Stegarescu, A.; Lung, I.; Ciorî, A.; Kacso, I.; Opri, O.; Soran, M.L.; Soran, A. The Antibacterial Properties of Nanocomposites Based on Carbon Nanotubes and Metal Oxides Functionalized with Azithromycin and Ciprofloxacin. *Nanomaterials* **2022**, *12*, 4115. [CrossRef]
69. Noor, M.M.; Santana-Pereira, A.L.R.; Liles, M.R.; Davis, V.A. Dispersant Effects on Single-Walled Carbon Nanotube Antibacterial Activity. *Molecules* **2022**, *27*, 1606. [CrossRef]
70. Jenkins, J.; Mantell, J.; Neal, C.; Gholinia, A.; Verkade, P.; Nobbs, A.H.; Su, B. Antibacterial effects of nanopillar surfaces are mediated by cell impedance, penetration and induction of oxidative stress. *Nat. Commun.* **2020**, *11*, 1626. [CrossRef]

71. Linklater, D.P.; De Volder, M.; Baulin, V.A.; Werner, M.; Jessl, S.; Golozar, M.; Maggini, L.; Rubanov, S.; Hanssen, E.; Juodkazis, S.; et al. High Aspect Ratio Nanostructures Kill Bacteria via Storage and Release of Mechanical Energy. *ACS Nano* **2018**, *12*, 6657–6667. [CrossRef]
72. Nie, C.; Cheng, C.; Ma, L.; Deng, J.; Zhao, C. Mussel-Inspired Antibacterial and Biocompatible Silver–Carbon Nanotube Composites: Green and Universal Nanointerfacial Functionalization. *Langmuir* **2016**, *32*, 5955–5965. [CrossRef]
73. Vecitis, C.D.; Zodrow, K.R.; Kang, S.; Elimelech, M. Electronic-Structure-Dependent Bacterial Cytotoxicity of Single-Walled Carbon Nanotubes. *ACS Nano* **2010**, *4*, 5471–5479. [CrossRef]
74. Abo-Neima, S.E.; Motaweh, H.A.; Elsehly, E.M. Antimicrobial activity of functionalised carbon nanotubes against pathogenic microorganisms. *IET Nanobiotechnol.* **2020**, *14*, 457–464. [CrossRef]
75. Liu, D.; Mao, Y.; Ding, L. Carbon nanotubes as antimicrobial agents for water disinfection and pathogen control. *J. Water Health* **2018**, *16*, 171–180. [CrossRef]
76. Nepal, D.; Balasubramanian, S.; Simonian, A.L.; Davis, V.A. Strong Antimicrobial Coatings: Single-Walled Carbon Nanotubes Armored with Biopolymers. *Nano Lett.* **2008**, *8*, 1896–1901. [CrossRef]
77. Hartono, M.R.; Kushmaro, A.; Chen, X.; Marks, R.S. Probing the toxicity mechanism of multiwalled carbon nanotubes on bacteria. *Env. Sci. Pollut. Res.* **2018**, *25*, 5003–5012. [CrossRef]
78. Rajavel, K.; Gomathi, R.; Manian, S.; Kumar, R.T.R. In Vitro Bacterial Cytotoxicity of CNTs: Reactive Oxygen Species Mediate Cell Damage Edges over Direct Physical Puncturing. *Langmuir* **2014**, *30*, 592–601. [CrossRef]
79. Sahoo, B.M.; Banik, B.K.; Borah, P.; Jain, A. Reactive Oxygen Species (ROS): Key Components in Cancer Therapies. *Anti-Cancer Agents Med. Chem.* **2022**, *2*, 215–222. [CrossRef]
80. Xie, W.; Zhang, S.; Pan, F.; Chen, S.; Zhong, L.; Wang, J.; Pei, X. Nanomaterial-based ROS-mediated strategies for combating bacteria and biofilms. *J. Mater. Res.* **2021**, *36*, 822–845. [CrossRef]
81. Kurilich, M.R.; Thapa, A.; Moilanen, A.; Miller, J.L.; Li, W.; Neupane, S. Comparative study of electron field emission from randomly-oriented and vertically-aligned carbon nanotubes synthesized on stainless steel substrates. *J. Vac. Sci. Technol. B Nanotechnol. Microelectron. Mater. Process. Meas. Phenom.* **2019**, *37*, 041202. [CrossRef]